Catastrophic ATP loss underlies a metabolic combination therapy tailored for *MYCN*-amplified neuroblastoma

Krista M. Dalton[a], Timothy L. Lochmann[a], Konstantinos V. Floros[a], Marissa L. Calbert[a], Richard Kurupi[a], Giovanna T. Stein[b,c], Joseph McClanaghan[b,c], Ellen Murchie[b,c], Regina K. Egan[b,c], Patricia Greninger[b,c], Mikhail Dozmorov[d], Sivapriya Ramamoorthy[e], Madhavi Puchalapalli[f], Bin Hu[f], Lisa Shock[g], Jennifer Koblinski[f], John Glod[h], Sosipatros A. Boikos[i], Cyril H. Benes[b,c,1], and Anthony C. Faber[a,1]

[a]Philips Institute for Oral Health Research, VCU School of Dentistry and Massey Cancer Center, Virginia Commonwealth University, Richmond, VA 23298; [b]Center for Cancer Research, Massachusetts General Hospital Cancer Center, Boston, MA 02129; [c]Department of Medicine, Harvard Medical School, Boston, MA 02115; [d]Department of Biostatistics, Virginia Commonwealth University, Richmond, VA 23298; [e]Discovery and Translational Sciences, Metabolon, Inc., Research Triangle Park, NC 27709; [f]Department of Pathology, Virginia Commonwealth University, Richmond, VA 23298; [g]Department of Microbiology and Immunology, Virginia Commonwealth University, Richmond, VA 23298; [h]Pediatric Oncology Branch, National Cancer Institute, National Institutes of Health, Bethesda, MD 20892; and [i]Department of Internal Medicine, Virginia Commonwealth University, Richmond, VA 23298

Edited by Robert N. Eisenman, Fred Hutchinson Cancer Research Center, Seattle, WA, and approved January 22, 2021 (received for review May 19, 2020)

***MYCN*-amplified neuroblastoma is a lethal subset of pediatric cancer. MYCN drives numerous effects in the cell, including metabolic changes that are critical for oncogenesis. The understanding that both compensatory pathways and intrinsic redundancy in cell systems exists implies that the use of combination therapies for effective and durable responses is necessary. Additionally, the most effective targeted therapies exploit an "Achilles' heel" and are tailored to the genetics of the cancer under study. We performed an unbiased screen on select metabolic targeted therapy combinations and correlated sensitivity with over 20 subsets of cancer. We found that *MYCN*-amplified neuroblastoma is hypersensitive to the combination of an inhibitor of the lactate transporter MCT1, AZD3965, and complex I of the mitochondrion, phenformin. Our data demonstrate that MCT4 is highly correlated with resistance to the combination in the screen and lowly expressed in *MYCN*-amplified neuroblastoma. Low MCT4 combines with high expression of the MCT2 and MCT1 chaperone CD147 in *MYCN*-amplified neuroblastoma, altogether conferring sensitivity to the AZD3965 and phenformin combination. The result is simultaneous disruption of glycolysis and oxidative phosphorylation, resulting in dramatic disruption of adenosine triphosphate (ATP) production, endoplasmic reticulum stress, and cell death. In mouse models of *MYCN*-amplified neuroblastoma, the combination was tolerable at concentrations where it shrank tumors and did not increase white-blood-cell toxicity compared to single drugs. Therefore, we demonstrate that a metabolic combination screen can identify vulnerabilities in subsets of cancer and put forth a metabolic combination therapy tailored for *MYCN*-amplified neuroblastoma that demonstrates efficacy and tolerability in vivo.**

neuroblastoma | MYCN | metabolomics | apoptosis | lactate

Despite their relative rarity compared to blood cancers, solid-tumor pediatric cancers are now the leading cause of pediatric cancer-related deaths. Among the most deadly is high-risk neuroblastoma (NB): amplification of *MYCN* confers high risk and is the clear driver of NB in these cancers (1). As such, MYCN remains the most important drug target in NB and one of the most important in pediatric cancer. Unfortunately, direct chemical targeting of MYCN has not yet been successful, and despite advancements in anti-GD2 immunotherapy (2), alternate ways of targeting *MYCN*-amplified NB may be needed to successfully treat this cancer.

One approach is to find tumor-specific vulnerabilities, which are exploitable pharmacologically. Many efforts, including ours (3), have exhaustively looked for kinase inhibitors with particular efficacy in *MYCN*-amplified NBs. However, the emerging picture is a lack of kinase inhibitor efficacy in *MYCN*-amplified NB. Other vulnerabilities may be classified under the broad category of drugs targeting epigenetic modifiers. For example, using a CRISPR/Cas9 screen, Stegmaier and colleagues demonstrated that *MYCN*-amplified NB may be susceptible to targeting the H3K27me methylase EZH2 (4); in a different study, they demonstrated the susceptibility of *MYCN*-amplified NB to the combination of BRD4 inhibitors with CDK7 inhibitors (5). In addition, Thiele and colleagues (6) demonstrated high-risk NBs were susceptible to inhibition of the lysine methyltransferase SETD8. As promising as these data are, it remains unknown whether tolerability and/or clinical activity in *MYCN*-amplified NB will occur and SETD8, BRD4, and CDK7 inhibitors so far are not in the pediatric clinic. Cell death inducers constitute a third category. To this point, we recently uncovered a susceptibility of *MYCN*-amplified NB to the BCL-2 inhibitor venetoclax (3), confirmed by others (7). There, MYCN-driven NOXA expression sensitizes cells to venetoclax (3).

Significance

High-risk neuroblastoma accounts for nearly 15% of all pediatric cancer-related deaths. MYCN is an oncogene amplified in roughly half of high-risk neuroblastoma cases and finding new therapies to neutralize MYCN is a high priority for pediatric cancer. Here we demonstrate that *MYCN*-amplified neuroblastomas are sensitive to the combined inhibition of MCT1 and complex I of the mitochondrion. Sensitivity is due to low expression of MCT4 and high expression of MCT1 and the MCT1 chaperone CD147. Pharmacologic inhibition with AZD3965 and phenformin leads to complementary inhibition of metabolic processes that ultimately leads to cell death.

Author contributions: C.H.B. and A.C.F. designed research; K.M.D., T.L.L., K.V.F., M.L.C., R.K., G.T.S., J.M., E.M., R.K.E., S.R., M.P., and B.H. performed research; M.D. and L.S. contributed new reagents/analytic tools; K.M.D., T.L.L., P.G., M.D., S.R., L.S., J.K., J.G., S.A.B., C.H.B., and A.C.F. analyzed data; K.M.D., T.L.L., M.D., L.S., J.K., J.G., S.A.B., C.H.B., and A.C.F. contributed to the interpretation of results and provided critical feedback; and K.M.D., T.L.L., C.H.B., and A.C.F. wrote the paper.

Competing interest statement: The work in the laboratory of C.H.B. is funded in part by Amgen and Novartis. A.C.F. has served as a paid consultant for AbbVie. Amgen, Novartis, and AbbVie had no role in the conceptualization, study design, data collection and analysis, decision to publish, or preparation of the manuscript.

This article is a PNAS Direct Submission.

[1]To whom correspondence may be addressed. Email: cyrilbenes@gmail.com or acfaber@vcu.edu.

This article contains supporting information online at https://www.pnas.org/lookup/suppl/doi:10.1073/pnas.2009620118/-/DCSupplemental.

Published March 24, 2021.

Venetoclax is now in early phase trials in pediatric patients including those with NB (NCT03236857). It remains to be seen whether or not it will elicit responses in NB patients as a single agent.

A fourth distinct category of therapeutic strategies to indirectly target oncogenes is through metabolism targeting, involving the growing coterie of drugs targeting the pathways fulfilling the high-energy demands of cancer cells. A major energy currency in cells is adenosine triphosphate (ATP). The Warburg effect describes the propensity of cancer cells (and highly proliferating normal cells) to produce ATP in the presence of oxygen with the less efficient, extramitochondrial glycolysis, as opposed to the more efficient mitochondria-based oxidative phosphorylation occurring in most noncancerous cells (8). The mechanistic explanation of the Warburg effect and how it might benefit cancer cells has been revised dramatically over the years. It was originally proposed that mitochondria from cancer cells were defective and lacked oxidative phosphorylation capabilities (9); on the contrary, emerging data show that many cancers rely on oxidative phosphorylation to facilitate the generation of ATP (8, 10). Interestingly, while amplified *MYCN* directly regulates the expression of many of the key glycolytic enzymes and as such contributes to the Warburg effect (11, 12), a study utilizing a Seahorse respirator demonstrated that a *MYCN*-amplified NB cell line favored oxidative phosphorylation over glycolysis for the metabolic needs, while the reverse was true for a *MYCN* wild-type NB cell line (13). In an independent study, MYCN was associated with higher glycolytic flux and oxidative phosphorylation and conferred sensitivity to fatty acid oxidation disruption (12). Overall, since c-MYC, which shares ∼40% binding homology to DNA-binding sites throughout the genome with MYCN, has been extensively characterized as a metabolic master regulator (14, 15), it is likely there are other MYCN-driven metabolic processes that may represent significant drug targets.

Monocarboxylate transporters (MCTs) consist of four members (MCT1–4) in mammalian cells. Among their most critical substrates are lactate and pyruvate; MCT1 and MCT4 are responsible for lactate export across the plasma membrane to the extracellular space (16). AZD3965 (17) (AstraZeneca) is the first in-class–specific MCT1/2 dual inhibitor and is currently in early phase trials for diverse cancers; however, other inhibitors from different companies have recently been developed as well (18). Of note, AZD3965 has demonstrated good tolerability in diverse patients (clinical trial number NCT01791595). Although rare (65 cases/100,000 person-years), lactic acidosis led to the market retrieval of phenformin in America (19), yet phenformin remains in use as a type II antidiabetic drug in Europe, functioning centrally as a mitochondrial complex I electron transport chain (ETC) inhibitor. Phenformin reduces both glycolytic intermediates and pyruvate, increases shunting of glucose-derived carbon (increasing total lactate production), and markedly reduces tricarboxylic acid cycle intermediates (20). Indeed, there has been a recent resurgence in interest in the use of phenformin to treat cancer. For example, in *BRAF* mutant melanoma, phenformin sensitized cells to BRAF inhibitor through cooperative suppression of the metabolic sensor pathway mTORC1 (21). These preclinical data have led to a clinical trial of phenformin in combination with BRAF inhibitor in *BRAF* mutant melanoma (NCT03026517). Overall, while targeting individual metabolic pathways has demonstrated some preclinical success in different cancer models, it is limited with significant redundancy in pathways to generate ATP and regenerate NAD+ (22). We therefore assessed potential combination therapies involving metabolic targeting drugs to identify a strategy for *MYCN*-amplified NB.

Results

High-Throughput Screening Reveals Sensitivity of AZD3965/Phenformin in *MYCN*-Amplified Neuroblastoma. The Genomics of Drug Sensitivity of Cancer (GDSC) is a comprehensive drug-screening platform aimed at discovering new drug sensitivities for genetically distinct subsets of cancer (23, 24). We have used this platform to generate targeted therapy strategies that are in the process of clinical trial testing (3, 25, 26), as well as epigenetic targeted therapy strategies (27). Here, we redesigned the platform to screen and capture sensitivities of metabolic-targeting drugs in

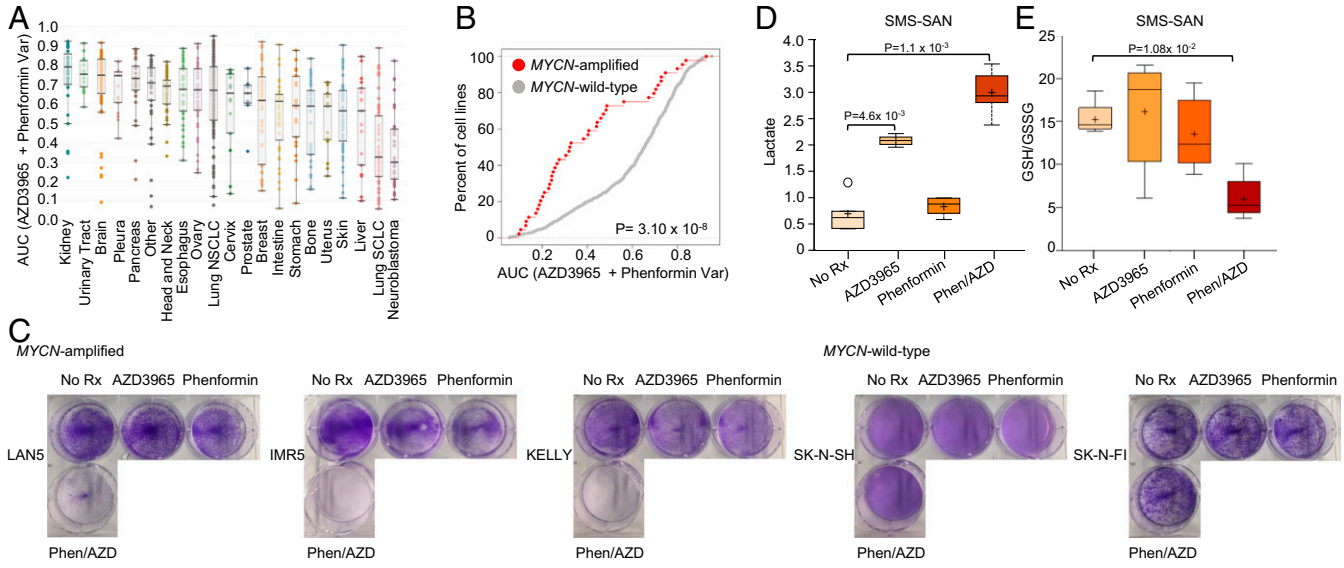

Fig. 1. *MYCN*-amplified neuroblastoma demonstrates sensitivity to AZD3965/phenformin. (*A*) Distribution of sensitivity across tissue of origin to the combination of AZD3965 and phenformin: AZD3965 (fixed dose of 128 nM) and phenformin (variable dose 2 μM to 7.8 nM). Area under the dose–response curve (AUC) is used as the metric for drug response. (*B*) Cumulative distribution of AUC values for *MYCN*-amplified versus *MYCN* wild-type cell lines from cancer subtypes listed in *A*. The values in *A* and *B* are from the GDSC drug-screening platform using resazurin to measure cell viability. (*C*) Long-term proliferation as measured by crystal violet assays over 5- to 7-d treatments with 1 μM AZD3965, 10 μM phenformin, or the combination in *MYCN*-amplified cell lines and *MYCN* wild-type cell lines. The SMS-SAN cells were treated with no drug, 1 μM AZD3965, 10 μM phenformin, or the combination of both drugs ($n = 5$ for all groups) for 48 h. Metabolic analysis was used to measure the level of (*D*) lactate and (*E*) GSH/GSSG ratio.

combinations of two. We here report the hypersensitivity of NB, and in particular of *MYCN*-amplified NB, to the combination of the MCT-1/2 inhibitor AZD3965 and the biguanide phenformin (Fig. 1 *A* and *B*, *SI Appendix*, Table S1, and Datasets S1 and S2). Confirming the robustness of the findings, the reverse combination using a fixed dose of phenformin added to a variable dose to AZD3965 yielded highly consistent results (*SI Appendix*, Figs. S1 and S2). Response to phenformin alone was not linked to MYCN status, while response to the MCT1 inhibitor alone was modestly linked to MYCN status compared to the strong association seen with the combination (*SI Appendix*, Figs. S1 and S2). Sensitivity to the combination of AZD3965 and phenformin was reproduced with AZD3965 and a chemically distinct complex I inhibitor, IACS-010759 (*SI Appendix*, Fig. S3*A*). To ensure that AZD3965 was on target, we silenced MCT1 with small interfering RNA (siRNA). Again, the combination of MCT1 siRNA and phenformin approximated the sensitivity seen with AZD3965 and phenformin (*SI Appendix*, Fig. S3 *B–G*). Similarly, the combination of MCT1 siRNA and IACS-010759 approximated AZD3965 and IACS-010759 (*SI Appendix*, Fig. S3 *B–G*). Altogether, these data demonstrate cotargeting of MCT1 and that complex I is effective in *MYCN*-amplified NB.

For the metabolic combinations in the GDSC screen, we utilized resazurin, which measures viability through several enzymatic activities in viable cells rather than ATP content (28). We corroborated the screen data of combination efficacy in the *MYCN*-amplified NB group using crystal violet assays, which intercalates with intact DNA and protein and is a reliable stain to quantify adherent cells independently of their metabolic status (29) (Fig. 1*C*). On the other hand, *MYCN* wild-type NBs were substantially less sensitive to the combination therapy (Fig. 1*C*). As different media formulas affect sensitivity to biguanides (30, 31), sensitivity to the combination therapy was tested using media containing either 1 mM pyruvate (Dulbecco's Modified Eagle Media [DMEM]/F12) or no pyruvate (RPMI). We found that the sensitivity patterns were consistent irrespective of the media used (*SI Appendix*, Fig. S4).

Intracellular lactic acid accumulation through disruption of MCT1 can be enhanced by biguanides (32, 33). We next utilized mass-spectrometry–based metabolite measurements in the *MYCN*-amplified SMS-SAN NB cells treated with single agents and the combination of AZD3965 and phenformin (Fig. 1 *D* and *E* and *SI Appendix*, Fig. S5). This experiment measured 655 metabolites following treatment with AZD3965, phenformin, or the combination, compared to untreated cells ($n = 5$ biological replicates for each condition; Dataset S3). In line with other studies, the combined blocking of MCT1 and mitochondrial complex I caused enhanced lactate accumulation (32, 33) in the SMS-SAN cells (Fig. 1*D*), leading to a high cellular level of oxidative stress, demonstrated through the ratio of reduced glutathione (GSH) to oxidized glutathione (GSSG) (Fig. 1*E*). Of note, we did not detect an increase in pyurvate (*SI Appendix*, Fig. S5), which in some instances may be elevated following MCT1/phenformin treatment (34).

The Presence of Amplified MYCN Sensitizes to AZD3965/Phenformin. Sensitivity correlated with *MYCN* amplification in the high-throughput screening (HTS) (Fig. 1*B*), which suggested that MYCN overexpression may mechanistically sensitize NBs to the combination of MCT1 and complex I inhibition. Our data demonstrated a highly stressed cell state (Fig. 1*E*) following lactate accumulation (Fig. 1*D*); this suggested a reduction in ATP, potentially through "feedback" shutdown of glycolysis caused by lactate accumulation, with the additional decrease of ATP caused by direct shutdown of oxidative phosphorylation by phenformin (16, 20, 32, 35). We therefore assayed a panel of *MYCN*-amplified NB cells to determine whether ATP was depleted following treatment. Indeed, the combination synergistically depleted ATP in the *MYCN*-amplified NB cell lines (Fig. 2*A*). To more directly assess the role of MYCN in this process, we employed syngenic cell-line pairs that expressed exogenous MYCN or expressed exogenous GFP as a control (3, 36). For these assays, cellular content in ATP was measured using CellTiter- Glo, which also is a quantitative assay for cellular viability within the proper cell concentrations (37). We found striking differences in the depletion of ATP by AZD3965 plus phenformin in RPE.1 cells, CHLA20 NB cells, and CHLA172 NB cells expressing MYCN compared to their GFP-expressing counterparts (Fig. 2*B*). When tested at a shorter time point (16 h), the combination therapy consistently decreased ATP levels (*SI Appendix*, Fig. S6*A*), demonstrating that depletion of ATP is an early event that precedes cell death (Fig. 3*A*). Massive ATP depletion at 16 h was demonstrated selectively in the cells with exogenous expression of MYCN and not GFP (*SI Appendix*, Fig. S6*B*), and, conversely, silencing of MYCN led to mitigation of ATP loss (*SI*

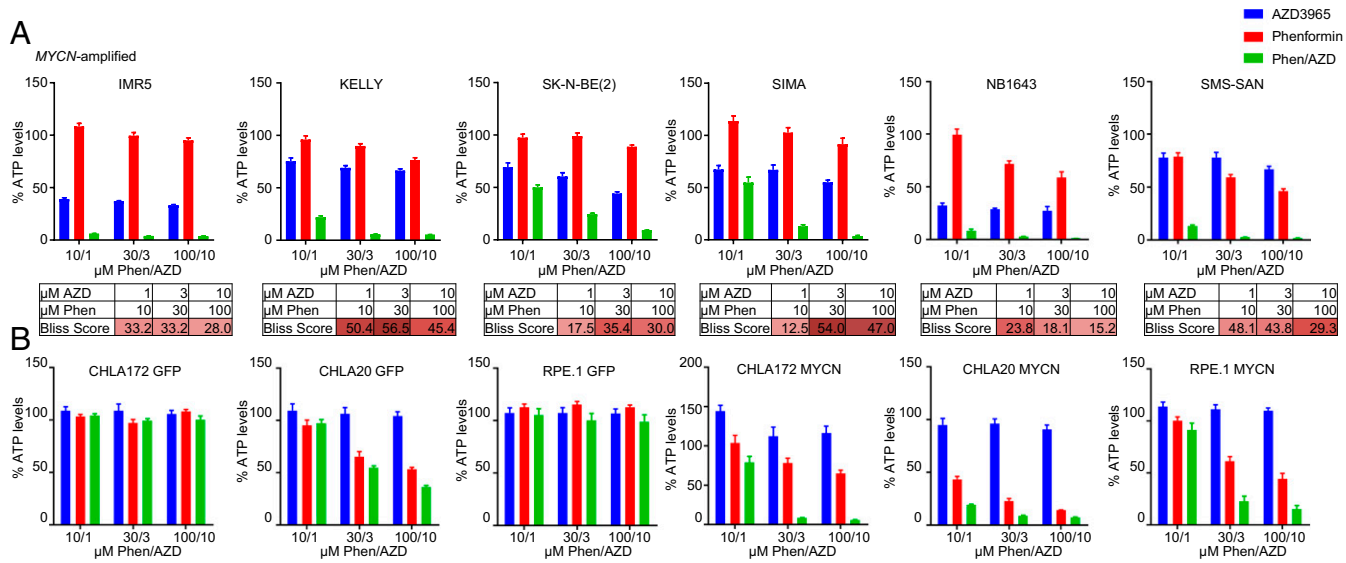

Fig. 2. AZD3965/phenformin synergizes in *MYCN*-amplified neuroblastoma. ATP/viability assay (CellTiter-Glo) was performed after a 72-h treatment of AZD3965 (1, 3, or 10 μM), phenformin (10, 30, or 100 μM), or the combination of both at the indicated concentrations for (*A*) *MYCN*-amplified cell lines analyzed by the Bliss synergy score (red indicates synergy, blue indicates antagonism) and (*B*) syngeneic cell-line pairs expressing exogenous MYCN or exogenous GFP as a control.

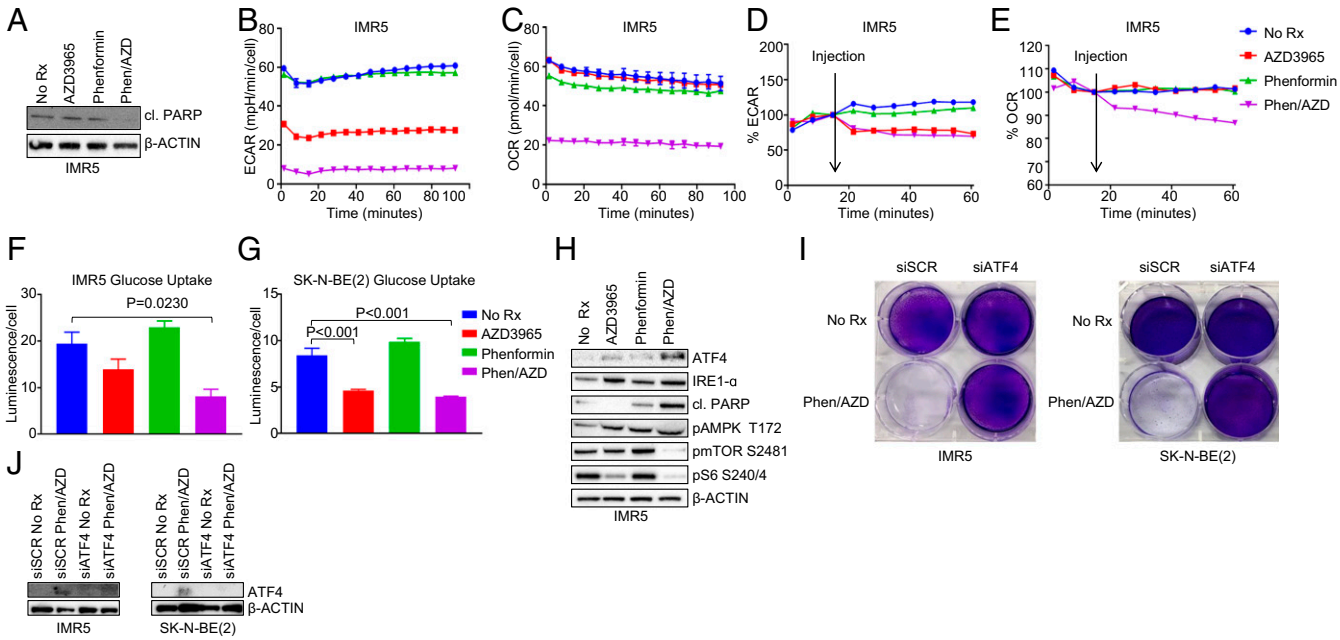

Fig. 3. AZD3965/phenformin affects metabolic function and induces apoptosis in *MYCN*-amplified neuroblastoma. (*A*) Western blotting measuring the levels of indicated proteins in the IMR5 cells treated with 1 μM AZD3965, 10 μM phenformin, or the combination of both for 16 h. The IMR5 cells were treated with 1 μM AZD3965, 10 μM phenformin, or the combination of both for 16 h, and their metabolic status was analyzed with the Seahorse XFp to measure (*B*) ECAR and (*C*) OCR. (*D*) The IMR5 cells were injected with 1 μM AZD3965, 10 μM phenformin, or the combination of both with (*D*) ECAR and (*E*) OCR measured immediately after injection with the Seahorse XFp. (*F*) The IMR5 and (*G*) SK-*N*-BE (2) cells were treated with 1 μM AZD3965, 10 μM phenformin, or the combination of both for 16 h, and glucose uptake was measured with Glucose Uptake-Glo assay. (*H*) Western blotting was used to detect the levels of the indicated antibodies in the IMR5 cells treated with 1 μM AZD3965, 10 μM phenformin, or the combination of both for 24 h. (*I*) Crystal violet assay of *MYCN*-amplified cell lines reverse-transfected with small interfering (si)-scramble or ATF4 siRNA treated for 5 to 7 d with 1 μM AZD3965 and 10 μM phenformin. (*J*) Western blot of *MYCN*-amplified cell lines reverse-transfected with si-scramble or ATF4 siRNA treated with 1 μM AZD3965 and 10 μM phenformin for 24 h and probed with the indicated antibodies.

Appendix, Fig. S7 *A* and *B*). Along with ATP levels, the ratio of ATP/ADP consistently decreased with the combination treatment of AZD3965 and phenformin only in the presence of MYCN (*SI Appendix*, Fig. S8*A*). As opposed to the low levels of sodium pyruvate (1 mM) in DMEM/F12 media, catastrophic loss of ATP could be partially restored with high levels (10 mM) of sodium pyruvate (*SI Appendix*, Fig. S8*B*), which corresponded to a concomitant partial rescue of toxicity (*SI Appendix*, Fig. S8 *C* and *D*). All these data are consistent with our hypothesis that sensitivity of the combination of AZD3965 plus phenformin is causatively linked to *MYCN* amplification status and occurs through a catastrophic loss of ATP.

ATP is primarily generated by glycolysis and oxidative phosphorylation. We next evaluated the state of glycolysis and oxidative phosphorylation following drug exposures. For these studies, we evaluated oxidative phosphorylation through oxygen consumption rate (OCR) and glycolysis through extracellular acidification rate (ECAR) on a Seahorse metabolic analyzer (32). We utilized the *MYCN*-amplified IMR5 cells instead of the SMS-SAN cells since these cells are fully adherent and more ideal for this assay. We found that AZD3965 was sufficient to decrease the extracellular acidification rate, which may be due to a decrease in glycolysis, while phenformin did not have any effect. As would be expected, the two combined to have a greater impact on glycolysis reduction than single agents (Fig. 3*B*). Impressively, while phenformin alone was sufficient to reduce oxidative phosphorylation, the two drugs combined to have a marked effect on oxidative phosphorylation (Fig. 3*C*). These metabolic effects, much like loss of ATP (*SI Appendix*, Fig. S6 *A* and *B*), were independent of cell death, which was yet not occurring at 16 h (Fig. 3*A*). Short-term analysis showed that, immediately upon injection, the combination of AZD3965 and phenformin reduced ECAR (Fig. 3*D*) and OCR (Fig. 3*E*) levels. Furthermore, consistent with decreased glycolytic flux, the combination therapy reduced glucose uptake (Fig. 3 *F* and *G*). These data are consistent with the markedly increased loss of ATP by both drugs upon overexpression of MYCN (Fig. 2*B* and *SI Appendix*, Fig. S6*B*). Loss of ATP is often counteracted by cells through increased AMPK activity to blunt the mTORC1 pathway. Indeed, we found active AMPK and deactivated mTORC1 (Fig. 3*H* and *SI Appendix*, Fig. S9*A*). In addition, in line with ATP catastrophic loss, we noted that cell death was most evident in the AZD3965 and phenformin combination treated cells based on cleaved PARP (Fig. 3*H* and *SI Appendix*, Fig. S9*B*). We also found increased presence of endoplasmic reticulum (ER) stress markers (Fig. 3*H* and *SI Appendix*, Fig. S9*A*) that mitigated loss of cell viability from the combination treatment when silenced (Fig. 3 *I* and *J*).

Amplified MYCN Modulates the Mitochondria in Neuroblastoma. We recently found that MYCN sensitizes cells to a BCL-2 inhibitor through transcriptional activation of the BH3-only protein NOXA (3). We reasoned that amplified *MYCN* was likely to cause hypersensitivity to AZD3965/phenformin through transcriptional changes. Recently, Brady et al. (38) have demonstrated that MYCN regulates mitochondrial genes in NB. We therefore examined RNA sequencing (RNA-seq) data (Gene Expression Omnibus [GEO] accession no. GSE80153) from a recent study (5) to analyze differences between MYCN high (mimicking *MYCN* amplification) and MYCN low NB. We used the DAVID tool (39) to analyze pathway differences from RNA-seq data between tet-off MYCN SHEP21N cells in the presence (tet-off/MYCN-on) and absence (tet-on/MYCN-off) of doxycycline. This unbiased analysis revealed mitochondrial-associated genes as the most up-regulated pathway in high MYCN (Fig. 4*A*). Further analyses of these genes demonstrated that complex I genes were the most

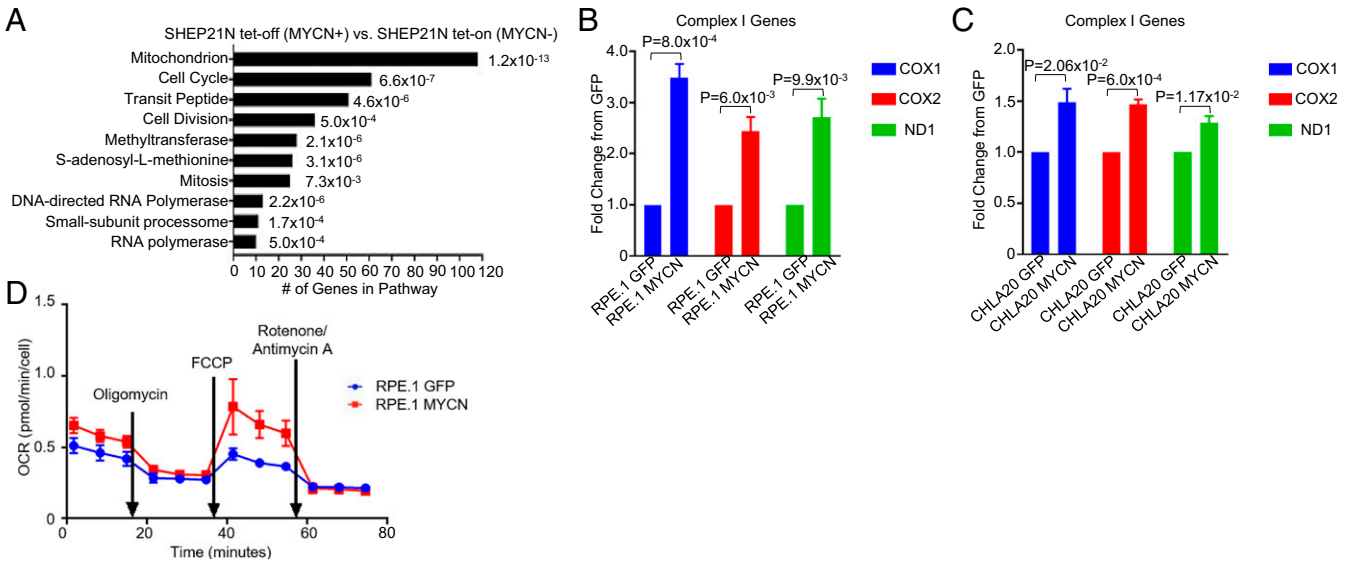

Fig. 4. The mitochondria is modified by amplified *MYCN* in neuroblastoma. (*A*) Gene expression data revealing differences in gene expression between the MYCN expressing and non-MYCN expressing SHEP21N cells. (*B* and *C*) The complex I gene expression fold change from the GFP-expressing RPE.1 and CHLA20 cells and the MYCN-expressing RPE.1 and CHLA20 cells. (*D*) The RPE.1 GFP- and MYCN-expressing cells were analyzed with a Seahorse XFp mitochondrial stress test to measure OCR.

broadly affected (~40% of complex I-related genes up-regulated in the tet-off MYCN-on cells). These data show strong metabolic perturbation upon MYCN overexpression, particularly affecting mitochondrial complex I. To further examine the connection between MYCN and mitochondrial complex I, we evaluated the expression of complex I genes in the RPE.1 and CHLA20 cells with exogenous expression of GFP or MYCN. Here, we found that expression of MYCN caused an increase in the expression of various complex I genes (Fig. 4 *B* and *C*).

While MYCN leads to up-regulation of glycolytic genes (11), a study utilizing a Seahorse metabolic analyzer demonstrated that a *MYCN*-amplified NB cell line favored oxidative phosphorylation (OCR) over glycolysis (ECAR) for their metabolic needs, while the reverse was true for a *MYCN* wild-type NB cell line (13). More recently, Oliynik et al. (12) demonstrated both enhanced ECAR and OCR in NB with amplified *MYCN* compared to NB without amplified *MYCN*. To better characterize MYCN in these two metabolic processes, we utilized the isogenic RPE.1 GFP and RPE.1 MYCN cells. We found that baseline ECAR and OCR measurements were not consistently higher in the RPE.1 MYCN cells (Fig. 4*D* and *SI Appendix*, Fig. S10). We next conducted a mitochondrial function test in which a series of compounds with specific effects on the mitochondrial ETC are used (40). We found a reproducibly marked difference in maximum oxidation rate (respiration) measured following addition of the mitochondrial uncoupler carbonyl cyanide-p-triflouromethoxyphenylhydrazon (40) (Fig. 4*D*), with a significantly increased reserve capacity (difference between baseline OCR levels and maximal OCR levels) in the RPE.1 MYCN cells compared to the GFP cells. Interestingly, the addition of the complex I inhibitor rotenone and complex III inhibitor antimycin led to a sharp decrease in oxidative consumption in the RPE.1 MYCN cells, which brought oxidative consumption rates back to those of the RPE.1 GFP cells. These data demonstrate that the presence of amplified *MYCN* increases the maximum capacity of mitochondrial respiration, which would be expected to give the cells a distinct survival advantage in cellular-stressed conditions (40). However, importantly, this advantage is lost following complex I/III inhibition, providing a clue that inhibiting complex I following cellular stress may be an important strategy to treat *MYCN*-amplified NB.

AZD3965/Phenformin Induce ER Stress in *MYCN*-Amplified NB. Metabolic pressure, for example, induced by glutamine deprivation, can induce ER stress, as evidenced by the activation of the unfolded protein response in *MYCN*-amplified NB (41). Our data demonstrate that the combination of AZD3965 and phenformin leads to a greatly oxidized cell state (Fig. 1*E*) in parallel with massive ATP loss (Fig. 2), likely a result of dual blockage of glycolysis and oxidative phosphorylation caused by lactate accumulation. We also saw increases in IRE1-α and ATF4 (Fig. 3*H* and *SI Appendix*, Fig. S9*A*), consistent with the stressed state caused by the combination (Fig. 1*D*). Importantly, knockdown of ATF4 was sufficient to mitigate drug efficacy (Fig. 3 *I* and *J*), underlying the role of ER stress to link ATP loss with toxicity.

MCT1 inhibition, however, based on our HTS of 1,000 cancer cell lines with the single-agent AZD3965, is not effective in most cancers (*SI Appendix*, Fig. S1). It is well known that the two primary lactate exporters are MCT1 (encoded by *SLC16A1*) and MCT4 (encoded by *SLC16A3*) and that MCT4 can rescue toxic effects of inhibiting MCT1 by maintaining lactate export (10, 18, 35). Indeed, it has been suggested previously that concomitant inhibition of MCT1 and MCT4 might be necessary for broad anticancer activity (35) but would also be likely accompanied by intolerable toxicities based on the ubiquitous role of these transporters.

We performed a multivariate regression analysis (elastic nets) (24) using genomic data available for the GDSC cell lines including gene expression data (42). This modeling showed that, across genes associated with sensitivity or resistance to the AZD3965/phenformin combination, expression of MCT4 was by far the strongest predictor of resistance to the combination (Fig. 5*A* and Datasets S4 and S5, MCT4 higher expression in less-sensitive cell lines). Interestingly, the weight associated with MCT4 expression in the linear regression model was even larger in the combination regression-based model than in that obtained for the single-agent AZD3965 MCT1 inhibitor, indicating that MCT4 expression explains even more the resistance to the combination than to the single-agent MCT1 inhibitor (Dataset S4). In aggregate, the results point to the key role of MCT4 expression in mediating resistance to the combination and thus to the importance of understanding the relationship between high MYCN expression and MCT4 expression.

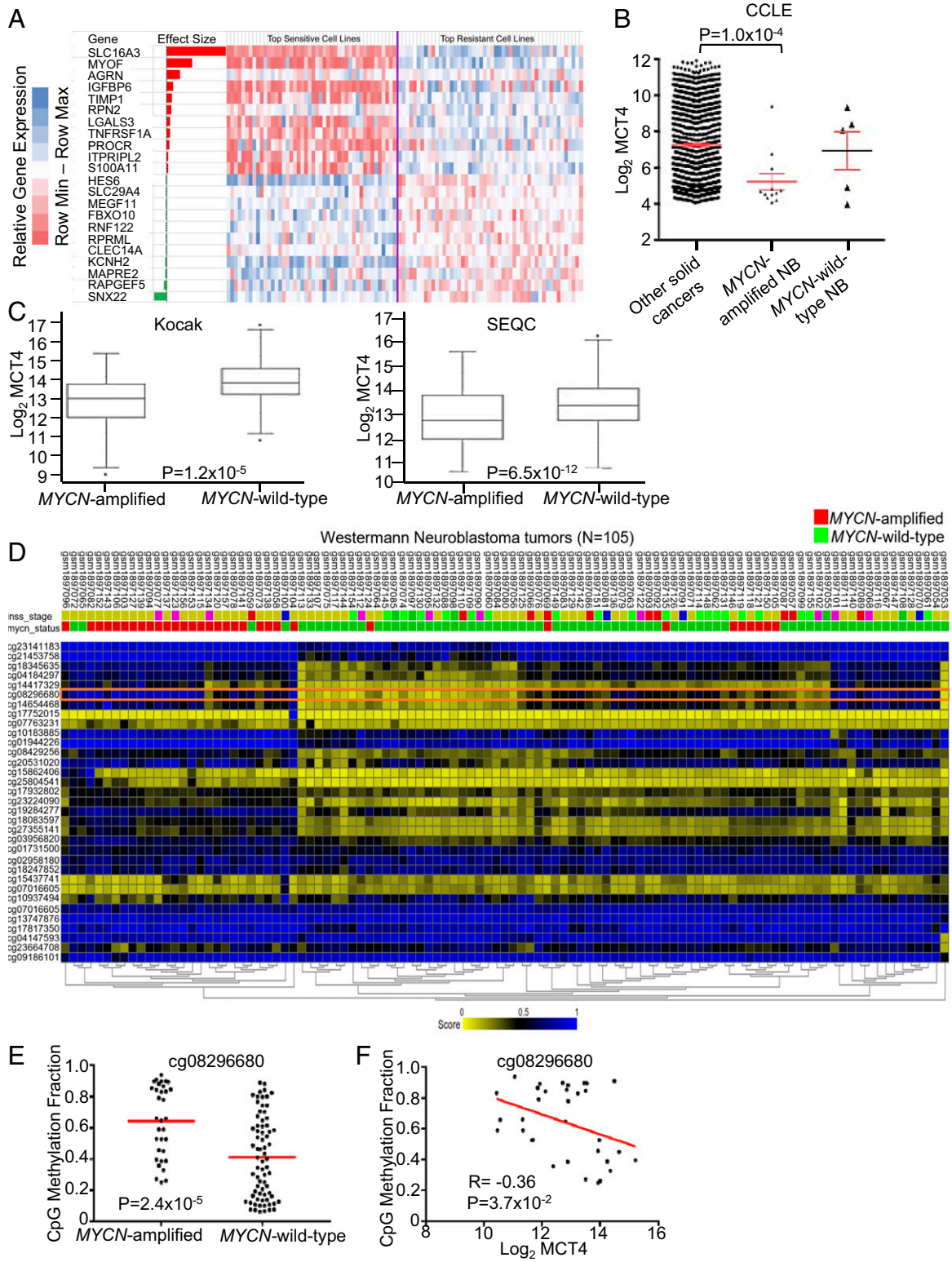

Fig. 5. MCT4 is heavily methylated in *MYCN*-amplified neuroblastoma. (*A*) Elastic net regression identifies genes associated with response to the MCT1 inhibitor plus phenformin combination. The genes with highest absolute effect are shown; the effect size corresponds to the importance of a given gene expression in the linear regression. MCT4 (SLC16A3) has the most weight in the model. The heatmap shows the relative expression of the corresponding genes in the 50 most-sensitive and the 50 least-sensitive cell lines (cell lines in between are omitted for display purposes). The gene expression levels are shown by indicated color scale. See Datasets S3 and S4 for the complete dataset. (*B*) MCT4 expression throughout cancer cell lines from CCLE. (*C*) MCT4 expression in *MYCN*-amplified neuroblastoma tumors ($n = 92$) compared to *MYCN* wild-type neuroblastoma tumors ($n = 401$) from the SEQC database and *MYCN*-amplified neuroblastoma tumors ($n = 93$) compared to *MYCN* wild-type neuroblastoma tumors ($n = 550$) from the Kocak database. (*D*) Analysis of MCT4 promoters in 105 neuroblastoma tumors. The orange rectangle highlights heavily methylated site in *MYCN*-amplified neuroblastoma tumors (cp08296680). (*E*) The CpG methylation fraction of site cp08296680 in *MYCN*-amplified compared to *MYCN* wild-type neuroblastoma tumors. (*F*) The correlation of CpG methylation fraction of site cp08296680 in *MYCN*-amplified neuroblastoma tumors with MCT4 expression.

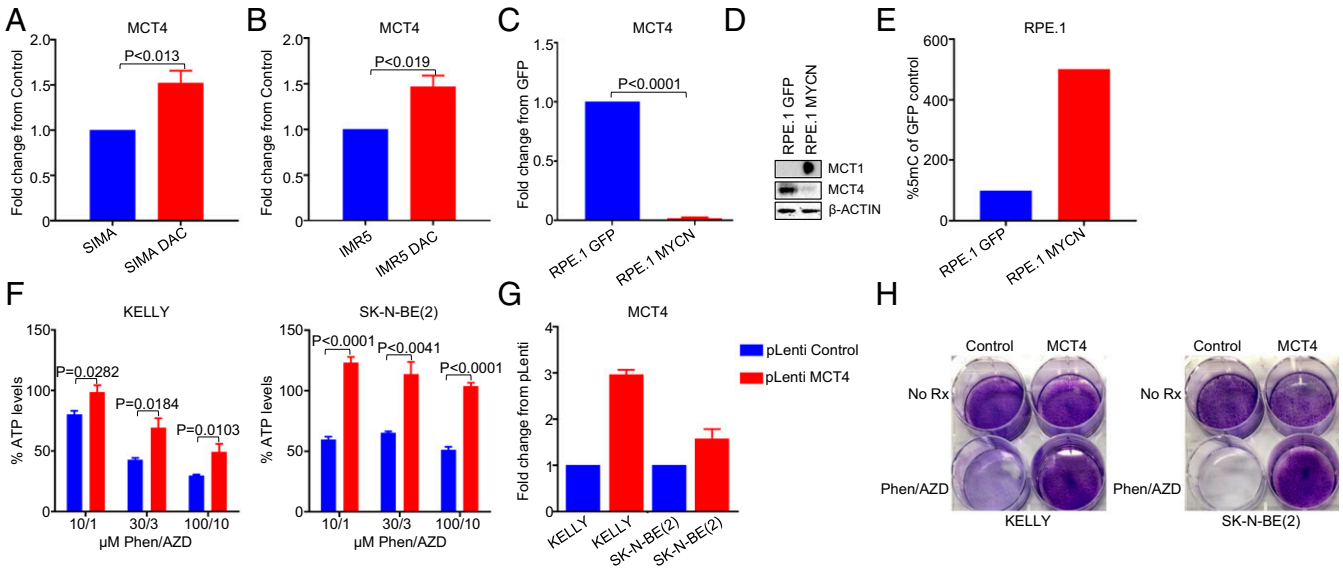

Fig. 6. MCT4 is related to a methylated phenotype and lowly expressed in *MYCN*-amplified neuroblastoma. The fold change of MCT4 gene expression from control in the *MYCN*-amplified (*A*) SIMA and (*B*) IMR5 cells treated with 1 μM decitabine for 72 h and RNA processed for qRT-PCR. (*C*) The fold change of MCT4 gene expression from the GFP-expressing RPE.1 cells and the MYCN-expressing RPE.1 cells. (*D*) Western blot of the GFP-expressing RPE.1 cells and the MYCN-expressing RPE.1 cells probed with the indicated antibodies. (*E*) The percentage of expression of 5-methylcytosine in the GFP-expressing RPE.1 cells compared to the MYCN-expressing RPE.1 cells. Transduction with pLenti control or pLenti MCT4 lentivirus in the *MYCN*-amplified cell lines KELLY and SK-*N*-BE (2) was performed and cells were assayed for (*F*) ATP/viability (CellTiter-Glo) following 16 h of treatment with AZD3965 (1, 3, or 10 μM), phenformin (10, 30, or 100 μM), or the combination at the indicated concentrations. (*G*) The fold-change of gene expression of MCT4 as determined by qRT-PCR and (*H*) a crystal violet assay following 5 to 7 d of treatment with the combination of 1 μM AZD3965 and 10 μM phenformin.

MCT4 Is Heavily Methylated in the *MYCN*-Amplified NB Subset. *MCT4* is located on chromosome 17 and is involved in the most common alteration in NB, partial 17q amplification (43); interestingly, it has long been known that 17q gain and *MYCN* amplification tend to co-occur (44). These data seem conflicting with MCT4 serving as the primary resistant mechanism for the combination and enhanced sensitivity among *MYCN*-amplified NB. To begin to evaluate this discrepancy, we determined MCT4 expression throughout cancer cell lines in an independent expression dataset, the Cancer Cell Line Encyclopedia (CCLE) dataset (45). In contrast to what was expected based on the amplification status but consistent with *MYCN*-amplified NB high sensitivity to MCT1 inhibition and combination of MCT1 inhibition and phenformin, we found that MCT4 expression was significantly lower in *MYCN*-amplified NB compared to all other cell lines, including *MYCN* wild-type NB (Fig. 5*B*). Analyses of NB tumors in two large public datasets confirmed the relationship between amplified *MYCN* and suppressed MCT4 in NB tumors (Fig. 5*C*).

One possible explanation for the discrepancy between gene copy and expression of MCT4 is that amplified *MYCN* either directly or indirectly suppresses MCT4 expression. Interestingly, analyses of the *MCT4* promoter in 105 annotated NB tumors demonstrated markedly altered methylation patterns in *MYCN*-amplified versus *MYCN* wild-type NB tumors (Fig. 5*D*). Upon further analyses, we found one such heavily methylated site in a large subset of *MYCN*-amplified NB tumors (cp08296680) (Fig. 5 *E* and *F*), supporting a role of methylation differences at the MCT4 promoter and gene in *MYCN*-amplified NB.

To analyze this further, we treated the *MYCN*-amplified NB cell lines SIMA and IMR5 with the DNA methyltransferase 1 (DNMT1) inhibitor decitabine (5′-Axa-2′deoxycytidine). MCT4 transcript levels increased, consistent with a methylated phenotype in *MYCN*-amplified NB (Fig. 6 *A* and *B*). MYCN has a predilection to bind to heavily methylated DNA (46) and correlates with methylation of different promoters in NB (47). Indeed, exogenous expression of MYCN in the RPE.1 model led to a sharp loss of MCT4 RNA and protein (Fig. 6 *C* and *D*), demonstrating a role of MYCN in decreased MCT4 expression. Consistently, methylation levels of RPE.1 were increased in the presence of MYCN (Fig. 6*E*). Altogether, these data demonstrate low MCT4 expression marked by differential methylation in *MYCN*-amplified NB tumors, which is at least in part regulated by MYCN. Consistently, overexpression of MCT4 with lentivirus-containing plasmids in the *MYCN*-amplified cell lines KELLY and SK-*N*-BE (2) led to marked mitigation of ATP loss and toxicity to the combination of AZD3965 and phenformin (Fig. 6 *F*–*H*).

***MYCN*-Amplified Neuroblastomas Have High Expression of CD147 and MCT1.** CD147 (basigin/emmprin) is a transmembrane glycoprotein that can bind diverse proteins and facilitate membrane delivery of specific proteins (48). CD147 acts as such a chaperone for MCT1 and regulates its expression at the protein level (49–51); knockout of CD147 was reported to result in a 10-fold loss of MCT1 activity (32), and the anticancer effects of inhibiting CD147 are largely attributed to its ability to enhance lactate accumulation (10). We therefore evaluated CD147 levels in NB. We found higher expression of CD147 in *MYCN*-amplified NB compared to NB without *MYCN* amplification across several datasets (Fig. 7*A*). Levels of MYCN and CD147 were correlated (52), and patients with high levels of CD147 had worse outcomes (Fig. 7*B*), and CD147 was increased in more advanced NB (Fig. 7*C*).

Similar to the data that we uncovered with CD147, MCT1 levels have recently been demonstrated to correlate with MYCN and to portend poor outcomes (53, 54). We found not only that MCT1 levels correlate with poor outcomes in NB (Fig. 7*D*), but also that high expression was sufficient to decrease survival probability in *MYCN* wild-type NB (Fig. 7*E*). Analyses of NB tumors in two large public datasets confirmed the correlation between CD147 and MCT1 (Fig. 7*F*).

MYCN Binds to the MCT1 Promoter to Up-Regulate It. We also found that MCT1 was higher, similar to CD147, in *MYCN*-amplified NB tumors (Fig. 8*A*). In the syngeneic lines, exogenous MYCN was sufficient to increase MCT1 expression (Fig. 8*B*) (52).

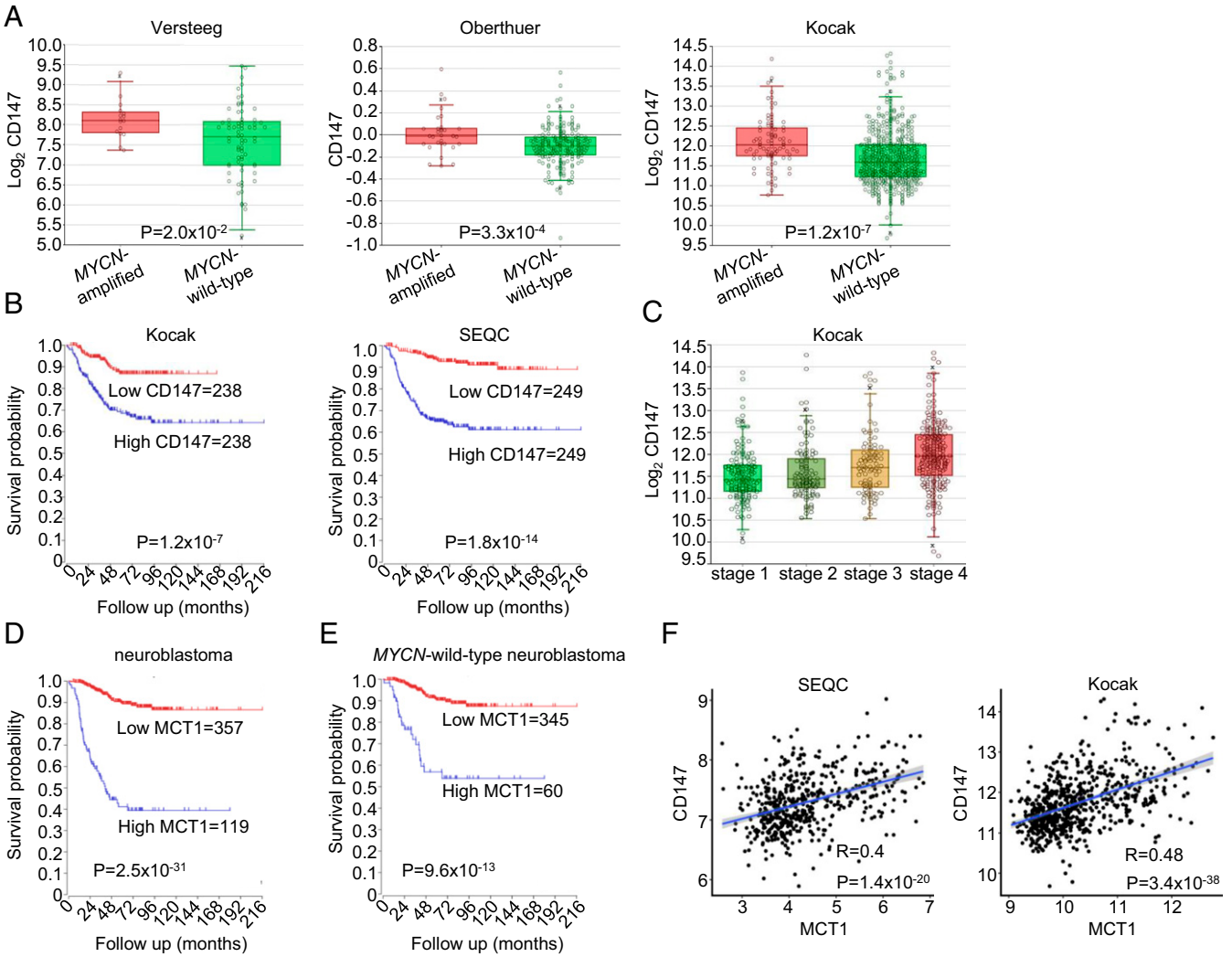

Fig. 7. High expression of CD147 and MCT1 in *MYCN*-amplified neuroblastoma. (*A*) The CD147 expression in *MYCN*-amplified neuroblastoma tumors ($n = 72$) compared to *MYCN* wild-type neuroblastoma tumors ($n = 16$) from the Versteeg database, *MYCN*-amplified neuroblastoma tumors ($n = 31$) compared to *MYCN* wild-type neuroblastoma tumors ($n = 220$) from the Oberthuer database, and *MYCN*-amplified neuroblastoma tumors ($n = 93$) compared to *MYCN* wild-type neuroblastoma tumors ($n = 550$) from the Kocak database. (*B*) The Kaplan curves for survival outcomes with high levels ($n = 236$) compared to low levels ($n = 235$) of CD147 from the Kocak database and survival outcomes with high levels ($n = 249$) compared to low levels ($n = 249$) of CD147 from the SEQC database. (*C*) The CD147 expression in neuroblastoma tumors separated by stage from the Kocak database. (*D*) The Kaplan curves for survival outcomes of all neuroblastoma tumors with high levels ($n = 119$) compared to low levels ($n = 357$) of MCT1 from the Kocak database. (*E*) Kaplan curves for the survival outcomes of *MYCN* wild-type neuroblastomas with high levels ($n = 60$) compared to low levels ($n = 345$) of MCT1 from the Kocak database. (*F*) The correlation of CD147 and MCT1 expression from the SEQC and Kocak databases as determined by linear regression analysis.

We next took advantage of a recent study (55) that examined MYCN binding throughout the genome in NB. We found from our analyses of MYCN at the *MCT1* promoter that, when MYCN was expressed in the SHEP21N cells, there was strong binding of MYCN to the *MCT1* promoter (Fig. 8*C*), which correlated with higher expression of MCT1 in the *MYCN*-expressing SHEP cells (Fig. 8*D*). We further corroborated these data in other *MYCN*-amplified NB cell lines (Fig. 8*C*). Importantly, read count peaks in the chromatin immunoprecipitation sequencing (ChIP-seq) data (Fig. 8*C*) correspond to E-BOX sites in the *MCT1* promoter, and sites were previously shown to be occupied by the related protein c-MYC in the P493-6 human B-cell lymphoma line (16). Consistent with the studies in the modified cell lines, analyses of 39 NB cell lines (56), which included most of the cell lines used in this study, corroborated our hypothesis that *MYCN*-amplified NBs have higher expression of MCT1 and lower expression of MCT4 (Fig. 8*E*). These data altogether demonstrate that MYCN binds to the *MCT1* promoter in NB to directly activate it and further sheds light on the relationship between MYCN and lactate handling in NB.

The Combination of AZD3965 and Phenformin Blocks Tumor Growth in *MYCN*-Amplified NB Mouse Models. We next sought to determine whether AZD3965/phenformin had in vivo activity. We first took advantage of several patient-derived xenograft (PDX) ex vivo models of *MYCN*-amplified NB (36, 56, 57) to more stringently evaluate the efficacy of this combination. As with the traditional *MYCN*-amplified cell lines, we uncovered robust synergistic activity of AZD3965/phenformin (Fig. 9*A*).

We therefore investigated the combination in mouse models. To do so, we utilized the SMS-SAN *MYCN*-amplified NB xenograft model (3) and the 561 PDX model (Fig. 9*A*). The doses used in this study were 100 mg/kg/qd/po AZD3965 and 100 mg/kg/qd/po phenformin, based on past studies (17, 21). We demonstrated over 2 wk that there was almost no effect of AZD3965 or phenformin alone on tumor growth in these models; however, the combination

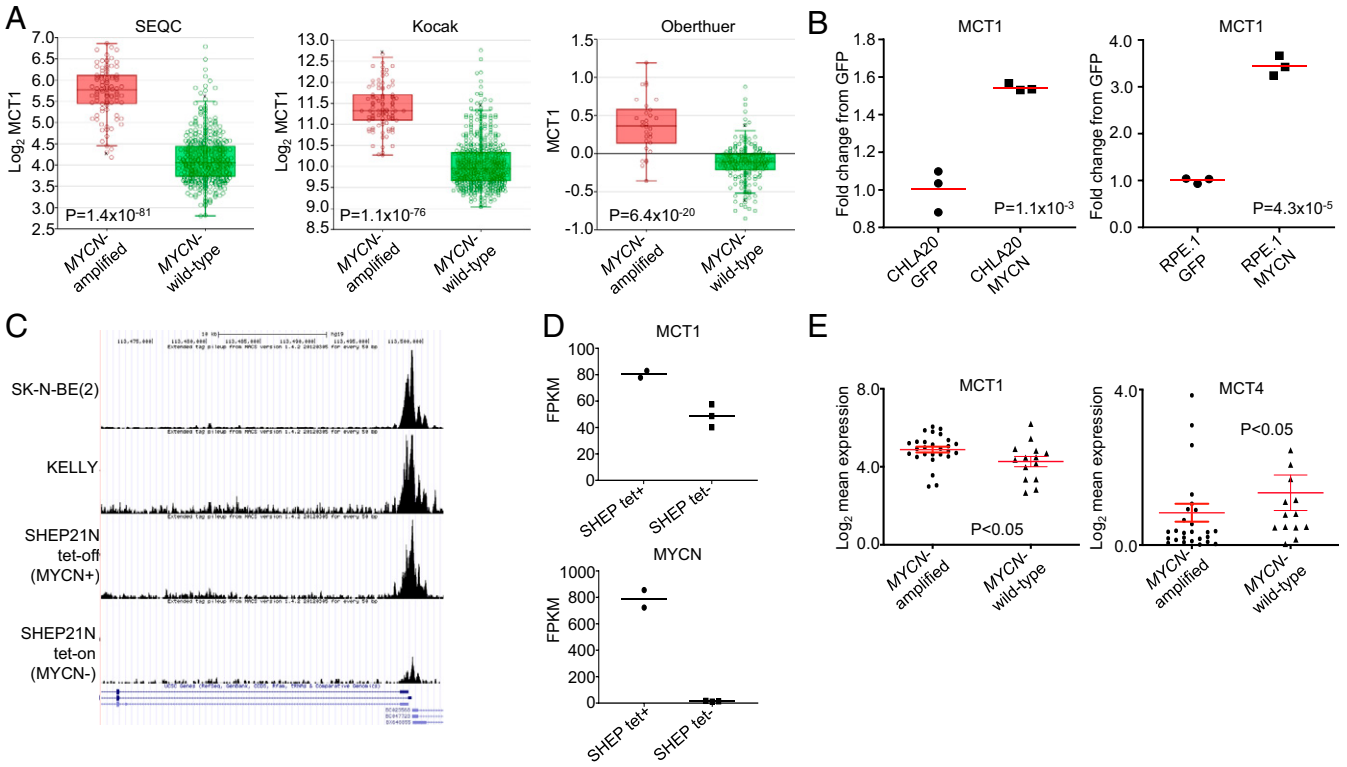

Fig. 8. High MCT1 expression in *MYCN*-amplified neuroblastoma. (*A*) The MCT1 expression in *MYCN*-amplified neuroblastoma tumors ($n = 92$) compared to *MYCN* wild-type neuroblastoma tumors ($n = 401$) from the SEQC database, *MYCN*-amplified neuroblastoma tumors ($n = 93$) compared to *MYCN* wild-type neuroblastoma tumors ($n = 550$) from the Kocak database and *MYCN*-amplified neuroblastoma tumors ($n = 31$) compared to *MYCN* wild-type neuroblastoma tumors ($n = 220$) from the Oberthuer database. (*B*) The MCT1 RNA expression from the CHLA20 GFP- expressing cells compared to the CHLA20 MYCN-expressing cells and the RPE.1 GFP-expressing cells compared to the RPE.1 MYCN-expressing cells as determined by qRT-PCR. (*C*) ChIP-seq of MYCN at the MCT1 promotor in *MYCN*-amplified NB cell lines, where read count peaks correspond to E-BOX sites in the *MCT1* promoter. (*D*) The MCT1 and MYCN expression in the MCYN-expressing and non-MYCN–expressing SHEP21N cells. (*E*) Expression of MCT1 and MCT4 in *MYCN*-amplified and *MCYN* wild-type neuroblastoma. For MCT4, two points outside this range are not shown for visual purposes.

blocked tumor growth in both models and shrank three of the six tumors in the SMS-SAN model (Fig. 9 *B*–*E*). This activity was obtained without obvious signs of toxicity (Fig. 9 *F* and *G*).

The Combination of AZD3965 and Phenformin Is Tolerable. Enhanced lactate accumulation would be expected to be toxic to most cells, likely at a unique threshold. While our mouse studies did not reveal any overt toxicity, we wanted to more thoroughly evaluate the effect of the combination at a dose sufficient to shrink *MYCN*-amplified NB. We conducted further toxicity studies in different blood populations to potentially uncover less overt toxicity (58). At the doses we used for the in vivo study, treatment with AZD3965, phenformin, or the combination of both did not lead to significant loss in red blood cells, white blood cells, neutrophils, reticulocytes, or platelets (Fig. 9*H*). Although the combination induced some depletion of lymphocytes, their level recovered fully after 24 h (Fig. 9*H*). These data imply a potential therapeutic window for this combination at doses where there is efficacy against NB; however, further evaluations such as in vivo metabolic profiling and liver- and kidney-function tests would be valuable.

Discussion

Targeting transcription factor oncogenes requires creativity beyond direct inhibitors. PROTACS (proteolysis targeting chimeras) may be important therapies in the future, as these have the ability to enrich degradation of transcription factors by the cellular machinery (59). Otherwise, targeting important downstream pathways—usually in combinations—is seen as a front-running strategy to incorporate small-molecule inhibitors.

In this study, we used a HTS of metabolic combinations to uncover a high sensitivity of *MYCN*-amplified NB to combined MCT1 and complex I inhibition. Sensitivity is underlined by several conspiring factors. First, MYCN directly up-regulates MCT1, the primary lactate importer into the cell, and, simultaneously, these cells have high expression of the MCT1 chaperone CD147. Second, *MYCN*-amplified NBs have heavily methylated MCT4, repressing its expression in NB and precluding functional redundancy with MCT1 (35). Indeed, in our combination screen of the MCT1 inhibitor AZD3965 and complex I inhibitor phenformin, MCT4 was the top-scoring resistant gene (with higher expression in resistant cell lines). Third, we found that MYCN greatly alters the mitochondrion. Among these changes, we noted an enhanced oxidative reservoir driven by MYCN; phenformin blocks this spare respiratory capacity, leading to massive loss of ATP in the presence of AZD3965, which is not seen in the absence of MYCN. Massive ATP loss leads to ER stress and death. These three factors likely combine to yield a potent effect of the combination in *MYCN*-amplified NB.

Numerous questions remain regarding the use of different metabolic pathways in *MYCN*-amplified NB. Interestingly, MYC- and MYCN-driven cancers, including NB, have a high rate of glutaminolysis (12, 60–62), which results in a high level of NADPH production (60) (and some ATP production as well), the former in line with increased nucleotide and fatty acid metabolism that has been reported for MYC-driven cancers (12, 63). Beyond a propensity for glutamine use, *MYCN*-amplified NBs are also glycolytic (12, 64), but how much more reliant on glycolysis are these tumors versus oxidative phosphorylation for their ATP needs

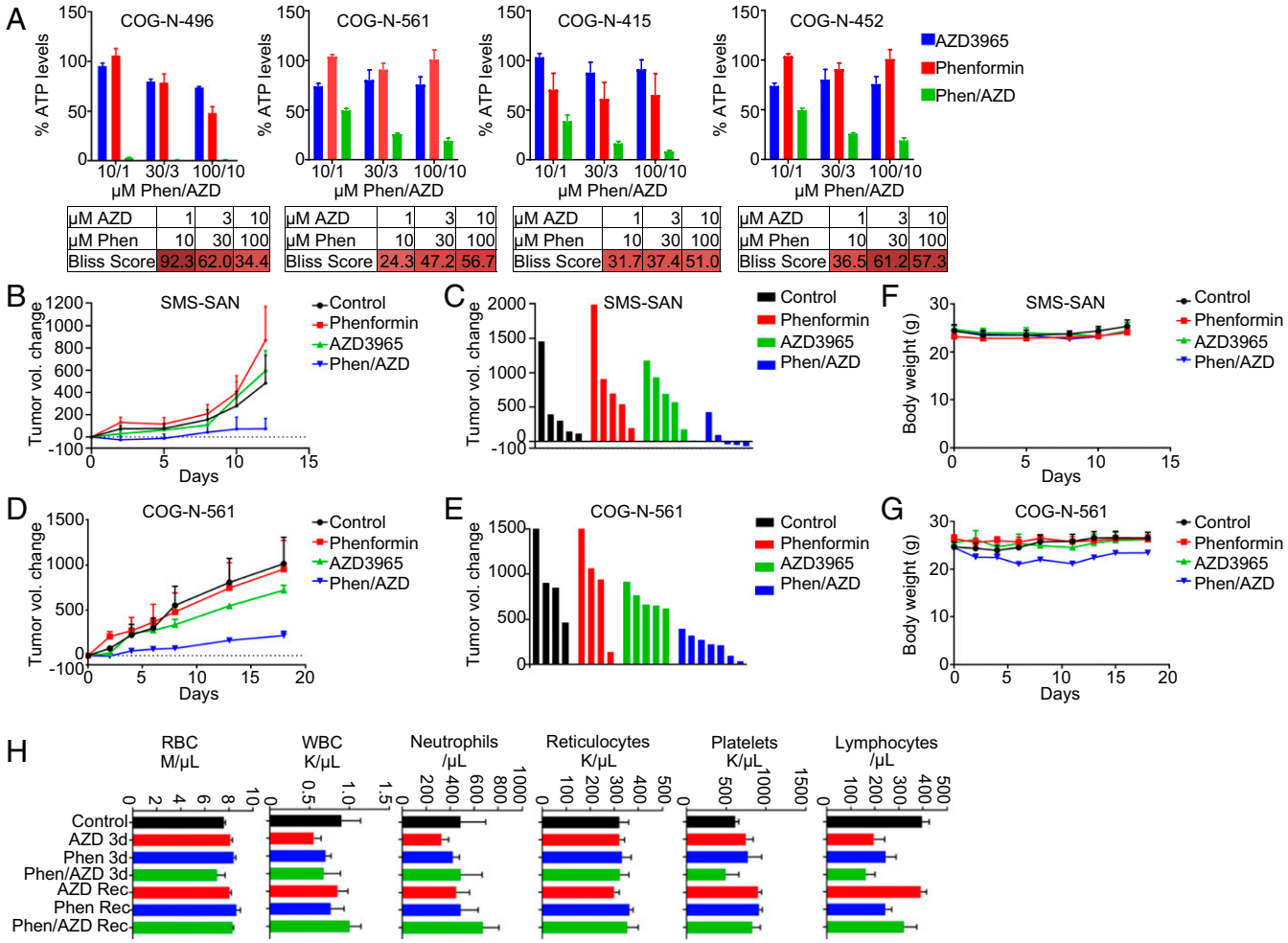

Fig. 9. The combination of AZD3965 and phenformin slows tumor growth in *MYCN*-amplified neuroblastoma mouse models. (*A*) ATP/viability assays were performed after 72 h of treatment with AZD3965 (1, 3, or 10 μM), phenformin (10, 30, 100 μM), or the combination at the indicated concentrations in PDX ex vivo cell cultures. (*B*) The SMS-SAN mouse model was treated with AZD3965, phenformin, or the combination of both 5 d/wk for 2 wk. (*C*) Volumetric change in individual tumor size from the start of treatment on day 12 for the SMS-SAN mouse model. (*D*) The COG-*N*-561 PDX mouse model was treated with AZD3965, phenformin, or the combination of both 5 d/wk for 2 wk. (*E*) Volumetric change in individual tumor size from start of treatment on day 18 for the COG-*N*-561 mouse model. (*F*) Body weight for the SMS-SAN mice. (*G*) Body weight for the COG-*N*-561 mice. (*H*) Mice were treated with no drug, AZD3965, phenformin, or the combination for 3 d before exsanguination, and the recovery (Rec) cohort was treated for 7 d and allowed 24 h of recovery from treatment before exsanguination.

remains unknown. While mitochondrial respiration activity has been reported to be down-regulated in NB (65), a recent report indicated they retain high oxidative phosphorylation activity (12). This appears difficult to reconcile, because *MYCN*-amplified NBs often have loss of the complex II subunit SDHB, mostly due to frequent concomitant *1p36* loss (66). However, it was reported that, when stressed, MYCN-driven NBs were able to increase the oxidative phosphorylation program in a way that was not seen without MYCN (12). The ability to increase oxidative phosphorylation under stress was also seen in our experiments where there was an increased oxidative reserve capacity (Fig. 4*B*). Therefore, it is likely that phenformin synergistically reduces ATP levels more dramatically in *MYCN*-amplified NBs compared to those without MYCN (Fig. 2), because it eliminates this protective stress response, negating what is likely a prominent survival advantage conferred by MYCN in NB. Further studies will be aimed at identifying how significant this oxidative stress response capacity is during the course of traditional therapies for neuroblastoma.

AZD3965 is currently in clinical trials for patients with diverse cancers (e.g., NCT01791595). MCT1 inhibition has demonstrated somewhat diverging results in different cancers and has the ability to down-regulate key glycolytic enzymes and increase intracellular lactate concentrations. Christofk and colleagues (34) found that MCT1 expression correlated with higher FDG avidity and a glycolytic phenotype, including up-regulation of MYC-driven glycolytic enzymes. However, intracellular lactate concentrations were not enhanced following MCT1 knockdown in breast cancer cells; nor did these investigators find decreased glycolytic flux, however, the investigators demonstrated increased oxidative consumption. Instead, anticancer effects were through blocking of pyruvate export.

We also found that MCT4 was heavily methylated in *MYCN*-amplified NB and that treatment with a DNMT1 inhibitor was sufficient to increase MCT4 expression. In addition, MYCN expression was sufficient to decrease MCT4 expression and increase global DNA methylation. MYCN has been revealed as having a repressive function for different genes including proapoptosis and genes involved in differentiation (67). As MYCN is a transcriptional amplifier and is not associated with de novo gene transcription (68), it is likely that MYCN does not directly repress genes, but, instead, increases the activation of epigenetic modifiers, for example, possibly DNMT1. Indeed, we are currently assessing the relationship between MYCN and DNMT1. These data imply that there may be a MYCN-driven epigenetic silencing of MCT4; however, more work is necessary to better understand this relationship.

Phenformin, despite being approved for use in humans in Europe, is no longer Food and Drug Administration approved in America. However, phenformin is being investigated in clinical trials as an anticancer agent (e.g., NCT03026517), where the toxicity profile has different metrics than it would have for antidiabetic medication. Lactic acidosis is the major concern for toxicity but appears mostly limited to diabetic patients with chronic renal failure (69). However, we found that toxicity of the combination was tolerable in our in vivo experiments; furthermore, we assayed blood populations at doses where there was marked antineuroblastoma activity. Blood cells were largely spared, and, importantly, toxicity was not exacerbated by the combination when compared to single-agent treatments (Fig. 9*H*). These metrics bode well for possible tolerance in human trials.

In conclusion, our data provide additional insights into how MYCN alters the metabolome and provides therapeutic opportunities for intervention. Blocking oxidative phosphorylation when *MYCN*-amplified NB tumors are stressed—with either MCT1 inhibition or otherwise—is an effective therapeutic approach in these cancers. Furthermore, blocking both glycolysis and oxidative phosphorylation simultaneously is particularly effective in cancer cells with amplified MYCN and can be achieved by enhancing lactate accumulation with MCT1 inhibitors in combination with mitochondrial targeting drugs like phenformin.

Materials and Methods

Cell Lines. The cell lines IMR5, SIMA, SMS-SAN, LAN5, NB1643, SK-N-BE(2), SK-N-SH, and KELLY were from the Molecular Center Therapeutics Laboratory at Massachusetts General Hospital, which performs routine testing of cell lines by single-nucleotide polymorphism and short tandem repeat analysis. The SK-N-FI cell line was provided by the Children's Hospital of Pennsylvania (Y. Mossé). The ex-vivo cells lines and corresponding in-vivo models COG-N-415, COG-N-496, COG-N-561, and COG-N-452, along with CHLA20 and CHLA172 cell lines were obtained from the Children's Oncology Group (COG) Cell Culture and Xenograft Repository. The SK-N-BE(2), SK-N-SH, IMR5, and SK-N-FI cell lines were regularly cultured in DMEM/F12 (50:50) supplemented with 10% fetal bovine serum (FBS). The RPE.1, SIMA, KELLY, NB1643, LAN5, and SMS-SAN cell lines were regularly cultured in RPMI 1640 supplemented with 10% FBS. The CHLA20 and CHLA172 cell lines were cultured in DMEM supplemented with 20% FBS and 1× insulin-transferrin-selenium (ITS); Thermo Fisher Scientific (catalog #41400045). The COG-N-415, COG-N-561, COG-N-452, and COG-N-496 cell lines were cultured in Iscove's modified Dulbecco's medium supplemented with 20% FBS and 1× ITS.

Drugs. AZD3965 and phenformin were purchased from Abmole for the nonscreening assays. IACS-010759 was purchased from Cayman Chemical. The drug stocks for the high-throughput drug screen were obtained from Selleck Chemicals.

Data Availability. All study data are included in the article and/or supporting information.

ACKNOWLEDGMENTS. We thank Dr. Yael Mossé (Children's Hospital of Philadelphia) for providing cell lines used in this study and Dr. C. Pat Reynolds and the Children's Oncology Group (COG) repository (Texas Tech University Health Sciences Center powered by Alex's Lemonade Stand Foundation) for providing neuroblastoma models. Services and products in support of the research project were generated by the Virginia Commonwealth University Massey Cancer Center Cancer Mouse Model Shared Resource, supported, in part, with funding from NIH/NCI Cancer Center Support Grant P30 CA016059. This work was also supported by the NCI Grants 1R01CA215610-01 (to A.C.F. and C.H.B.) and 1R01CA249219-01 (to A.C.F.).

1. M. Huang, W. A. Weiss, Neuroblastoma and MYCN. *Cold Spring Harb. Perspect. Med.* **3**, a014415 (2013).
2. M. E. Keyel, C. P. Reynolds, Spotlight on dinutuximab in the treatment of high-risk neuroblastoma: Development and place in therapy. *Biologics* **13**, 1–12 (2018).
3. J. Ham *et al*., Exploitation of the apoptosis-primed state of MYCN-amplified neuroblastoma to develop a potent and specific targeted therapy combination. *Cancer Cell* **29**, 159–172 (2016).
4. L. Chen *et al*., CRISPR-Cas9 screen reveals a MYCN-amplified neuroblastoma dependency on EZH2. *J. Clin. Invest.* **128**, 446–462 (2018).
5. A. D. Durbin *et al*., Selective gene dependencies in MYCN-amplified neuroblastoma include the core transcriptional regulatory circuitry. *Nat. Genet.* **50**, 1240–1246 (2018).
6. V. Veschi *et al*., Epigenetic siRNA and chemical screens identify SETD8 inhibition as a therapeutic strategy for p53 activation in high-risk neuroblastoma. *Cancer Cell* **31**, 50–63 (2017).
7. L. T. Bate-Eya *et al*., High efficacy of the BCL-2 inhibitor ABT199 (venetoclax) in BCL-2 high-expressing neuroblastoma cell lines and xenografts and rational for combination with MCL-1 inhibition. *Oncotarget* **7**, 27946–27958 (2016).
8. N. S. Akins, T. C. Nielson, H. V. Le, Inhibition of glycolysis and glutaminolysis: An emerging drug discovery approach to combat cancer. *Curr. Top. Med. Chem.* **18**, 494–504 (2018).
9. J. Zheng, Energy metabolism of cancer: Glycolysis versus oxidative phosphorylation (Review). *Oncol. Lett.* **4**, 1151–1157 (2012).
10. R. Le Floch *et al*., CD147 subunit of lactate/H+ symporters MCT1 and hypoxia-inducible MCT4 is critical for energetics and growth of glycolytic tumors. *Proc. Natl. Acad. Sci. U.S.A.* **108**, 16663–16668 (2011).
11. G. Qing *et al*., Combinatorial regulation of neuroblastoma tumor progression by N-Myc and hypoxia inducible factor HIF-1alpha. *Cancer Res.* **70**, 10351–10361 (2010).
12. G. Oliynyk *et al*., MYCN-enhanced oxidative and glycolytic metabolism reveals vulnerabilities for targeting neuroblastoma. *iScience* **21**, 188–204 (2019).
13. D. J. Smith, L. R. Cossins, I. Hatzinisiriou, M. Haber, P. Nagley, Lack of correlation between MYCN expression and the Warburg effect in neuroblastoma cell lines. *BMC Cancer* **8**, 259 (2008).
14. H. Shim *et al*., c-Myc transactivation of LDH-A: Implications for tumor metabolism and growth. *Proc. Natl. Acad. Sci. U.S.A.* **94**, 6658–6663 (1997).
15. A. L. Hsieh, Z. E. Walton, B. J. Altman, Z. E. Stine, C. V. Dang, MYC and metabolism on the path to cancer. *Semin. Cell Dev. Biol.* **43**, 11–21 (2015).
16. J. R. Doherty *et al*., Blocking lactate export by inhibiting the Myc target MCT1 disables glycolysis and glutathione synthesis. *Cancer Res.* **74**, 908–920 (2014).
17. B. M. Bola *et al*., Inhibition of monocarboxylate transporter-1 (MCT1) by AZD3965 enhances radiosensitivity by reducing lactate transport. *Mol. Cancer Ther.* **13**, 2805–2816 (2014).
18. M. Quanz *et al*., Preclinical efficacy of the novel monocarboxylate transporter 1 inhibitor BAY-8002 and associated markers of resistance. *Mol. Cancer Ther.* **17**, 2285–2296 (2018).
19. R. I. Misbin, Phenformin-associated lactic acidosis: Pathogenesis and treatment. *Ann. Intern. Med.* **87**, 591–595 (1977).
20. A. Janzer *et al*., Metformin and phenformin deplete tricarboxylic acid cycle and glycolytic intermediates during cell transformation and NTPs in cancer stem cells. *Proc. Natl. Acad. Sci. U.S.A.* **111**, 10574–10579 (2014).
21. P. Yuan *et al*., Phenformin enhances the therapeutic benefit of BRAF(V600E) inhibition in melanoma. *Proc. Natl. Acad. Sci. U.S.A.* **110**, 18226–18231 (2013).
22. S. Cassim, M. Vučetić, M. Ždralević, J. Pouyssegur, Warburg and beyond: The power of mitochondrial metabolism to collaborate or replace fermentative glycolysis in cancer. *Cancers (Basel)* **12**, 1119 (2020).
23. W. Yang *et al*., Genomics of drug sensitivity in cancer (GDSC): A resource for therapeutic biomarker discovery in cancer cells. *Nucleic Acids Res.* **41**, D955–D961 (2013).
24. M. J. Garnett *et al*., Systematic identification of genomic markers of drug sensitivity in cancer cells. *Nature* **483**, 570–575 (2012).
25. A. C. Faber *et al*., mTOR inhibition specifically sensitizes colorectal cancers with KRAS or BRAF mutations to BCL-2/BCL-XL inhibition by suppressing MCL-1. *Cancer Discov.* **4**, 42–52 (2014).
26. A. C. Faber *et al*., Assessment of ABT-263 activity across a cancer cell line collection leads to a potent combination therapy for small-cell lung cancer. *Proc. Natl. Acad. Sci. U.S.A.* **112**, E1288–E1296 (2015).
27. R. Hashizume *et al*., Pharmacologic inhibition of histone demethylation as a therapy for pediatric brainstem glioma. *Nat. Med.* **20**, 1394–1396 (2014).
28. J. O'Brien, I. Wilson, T. Orton, F. Pognan, Investigation of the Alamar Blue (resazurin) fluorescent dye for the assessment of mammalian cell cytotoxicity. *Eur. J. Biochem.* **267**, 5421–5426 (2000).
29. M. Feoktistova, P. Geserick, M. Leverkus, Crystal violet assay for determining viability of cultured cells. *Cold Spring Harb. Protoc.* **2016**, pdb prot087379 (2016).
30. K. Birsoy *et al*., Metabolic determinants of cancer cell sensitivity to glucose limitation and biguanides. *Nature* **508**, 108–112 (2014).
31. D. Y. Gui *et al*., Environment dictates dependence on mitochondrial complex I for NAD+ and aspartate production and determines cancer cell sensitivity to metformin. *Cell Metab.* **24**, 716–727 (2016).
32. I. Marchiq, R. Le Floch, D. Roux, M. P. Simon, J. Pouyssegur, Genetic disruption of lactate/H+ symporters (MCTs) and their subunit CD147/BASIGIN sensitizes glycolytic tumor cells to phenformin. *Cancer Res.* **75**, 171–180 (2015).
33. S. Granja *et al*., Disruption of BASIGIN decreases lactic acid export and sensitizes non-small cell lung cancer to biguanides independently of the LKB1 status. *Oncotarget* **6**, 6708–6721 (2015).
34. C. S. Hong *et al*., MCT1 modulates cancer cell pyruvate export and growth of tumors that co-express MCT1 and MCT4. *Cell Rep.* **14**, 1590–1601 (2016).
35. D. Benjamin *et al*., Dual inhibition of the lactate transporters MCT1 and MCT4 is synthetic lethal with metformin due to NAD+ depletion in cancer cells. *Cell Rep.* **25**, 3047–3058.e4 (2018).
36. T. L. Lochmann *et al*., Targeted inhibition of histone H3K27 demethylation is effective in high-risk neuroblastoma. *Sci. Transl. Med.* **10**, eaao4680 (2018).
37. M. Kijanska, J. Kelm, "In vitro 3D spheroids and microtissues: ATP-based cell viability and toxicity assays" in *Assay Guidance Manual*, G. S. Sittampalam *et al*., Eds. (Eli Lilly & Company, Bethesda, MD, 2004).

38. S. W. Brady *et al*., Pan-neuroblastoma analysis reveals age- and signature-associated driver alterations. *Nat. Commun.* **11**, 5183 (2020).
39. D. W. Huang, B. T. Sherman, R. A. Lempicki, Systematic and integrative analysis of large gene lists using DAVID bioinformatics resources. *Nat. Protoc.* **4**, 44–57 (2009).
40. F. Vazquez *et al*., PGC1α expression defines a subset of human melanoma tumors with increased mitochondrial capacity and resistance to oxidative stress. *Cancer Cell* **23**, 287–301 (2013).
41. S. Cardaci *et al*., Glutamine deprivation enhances antitumor activity of 3-bromopyruvate through the stabilization of monocarboxylate transporter-1. *Cancer Res.* **72**, 4526–4536 (2012).
42. F. Iorio *et al*., A landscape of pharmacogenomic interactions in cancer. *Cell* **166**, 740–754 (2016).
43. J. Vandesompele *et al*., Identification of 2 putative critical segments of 17q gain in neuroblastoma through integrative genomics. *Int. J. Cancer* **122**, 1177–1182 (2008).
44. S. O'Neill *et al*., MYCN amplification and 17q in neuroblastoma: Evidence for structural association. *Genes Chromosomes Cancer* **30**, 87–90 (2001).
45. J. Barretina *et al*., The Cancer Cell Line Encyclopedia enables predictive modelling of anticancer drug sensitivity. *Nature* **483**, 603–607 (2012).
46. D. M. Murphy *et al*., Global MYCN transcription factor binding analysis in neuroblastoma reveals association with distinct E-box motifs and regions of DNA hypermethylation. *PLoS One* **4**, e8154 (2009).
47. A. Decock *et al*., Genome-wide promoter methylation analysis in neuroblastoma identifies prognostic methylation biomarkers. *Genome Biol.* **13**, R95 (2012).
48. T. Muramatsu, Basigin (CD147), a multifunctional transmembrane glycoprotein with various binding partners. *J. Biochem.* **159**, 481–490 (2016).
49. D. K. Walters, B. K. Arendt, D. F. Jelinek, CD147 regulates the expression of MCT1 and lactate export in multiple myeloma cells. *Cell Cycle* **12**, 3175–3183 (2013).
50. W. Schneiderhan *et al*., CD147 silencing inhibits lactate transport and reduces malignant potential of pancreatic cancer cells in in vivo and in vitro models. *Gut* **58**, 1391–1398 (2009).
51. J. Su, X. Chen, T. Kanekura, A CD147-targeting siRNA inhibits the proliferation, invasiveness, and VEGF production of human malignant melanoma cells by down-regulating glycolysis. *Cancer Lett.* **273**, 140–147 (2009).
52. A. Bandino, D. Geerts, J. Koster, A. S. Bachmann, Deoxyhypusine synthase (DHPS) inhibitor GC7 induces p21/Rb-mediated inhibition of tumor cell growth and DHPS expression correlates with poor prognosis in neuroblastoma patients. *Cell Oncol. (Dordr.)* **37**, 387–398 (2014).
53. J. Fang *et al*., The H+-linked monocarboxylate transporter (MCT1/SLC16A1): A potential therapeutic target for high-risk neuroblastoma. *Mol. Pharmacol.* **70**, 2108–2115 (2006).
54. A. Khan *et al*., Targeting metabolic activity in high-risk neuroblastoma through monocarboxylate transporter 1 (MCT1) inhibition. *Oncogene* **39**, 3555–3570 (2020).
55. R. Zeid *et al*., Enhancer invasion shapes MYCN-dependent transcriptional amplification in neuroblastoma. *Nat. Genet.* **50**, 515–523 (2018).
56. J. L. Harenza *et al*., Transcriptomic profiling of 39 commonly-used neuroblastoma cell lines. *Sci. Data* **4**, 170033 (2017).
57. T. H. Nguyen *et al*., Fenretinide via NOXA induction, enhanced activity of the BCL-2 inhibitor venetoclax in high BCL-2-expressing neuroblastoma preclinical models. *Mol. Cancer Ther.* **18**, 2270–2282 (2019).
58. D. A. R. Heisey *et al*., The Ewing family of tumors rely on BCL-2 and BCL-XL to escape PARP inhibitor toxicity. *Clin. Cancer Res.* **25**, 1664–1675 (2018).
59. M. Konstantinidou *et al*., PROTACs: A game-changing technology. *Expert Opin. Drug Discov.* **14**, 1255–1268 (2019).
60. D. R. Wise *et al*., Myc regulates a transcriptional program that stimulates mitochondrial glutaminolysis and leads to glutamine addiction. *Proc. Natl. Acad. Sci. U.S.A.* **105**, 18782–18787 (2008).
61. G. Qing *et al*., ATF4 regulates MYC-mediated neuroblastoma cell death upon glutamine deprivation. *Cancer Cell* **22**, 631–644 (2012).
62. T. Wang *et al*., MYCN drives glutaminolysis in neuroblastoma and confers sensitivity to an ROS augmenting agent. *Cell Death Dis.* **9**, 220 (2018).
63. Z. E. Stine, Z. E. Walton, B. J. Altman, A. L. Hsieh, C. V. Dang, MYC, metabolism, and cancer. *Cancer Discov.* **5**, 1024–1039 (2015).
64. B. H. Kushner, H. W. Yeung, S. M. Larson, K. Kramer, N. K. Cheung, Extending positron emission tomography scan utility to high-risk neuroblastoma: Fluorine-18 fluorodeoxyglucose positron emission tomography as sole imaging modality in follow-up of patients. *J. Clin. Oncol.* **19**, 3397–3405 (2001).
65. R. G. Feichtinger *et al*., Low aerobic mitochondrial energy metabolism in poorly- or undifferentiated neuroblastoma. *BMC Cancer* **10**, 149 (2010).
66. J. García-López *et al*., Large 1p36 deletions affecting Arid1a locus facilitate mycn-driven oncogenesis in neuroblastoma. *Cell Rep.* **30**, 454–464.e5 (2020).
67. S. Gherardi, E. Valli, D. Erriquez, G. Perini, MYCN-mediated transcriptional repression in neuroblastoma: The other side of the coin. *Front. Oncol.* **3**, 42 (2013).
68. S. He, Z. Liu, D. Y. Oh, C. J. Thiele, MYCN and the epigenome. *Front. Oncol.* **3**, 1 (2013).
69. G. Enia, M. Garozzo, C. Zoccali, Lactic acidosis induced by phenformin is still a public health problem in Italy. *BMJ* **315**, 1466–1467 (1997).